

RSC Advances



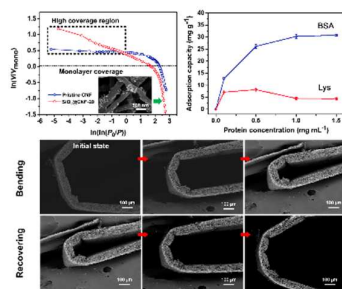
This is an *Accepted Manuscript*, which has been through the Royal Society of Chemistry peer review process and has been accepted for publication.

Accepted Manuscripts are published online shortly after acceptance, before technical editing, formatting and proof reading. Using this free service, authors can make their results available to the community, in citable form, before we publish the edited article. This *Accepted Manuscript* will be replaced by the edited, formatted and paginated article as soon as this is available.

You can find more information about *Accepted Manuscripts* in the [Information for Authors](#).

Please note that technical editing may introduce minor changes to the text and/or graphics, which may alter content. The journal's standard [Terms & Conditions](#) and the [Ethical guidelines](#) still apply. In no event shall the Royal Society of Chemistry be held responsible for any errors or omissions in this *Accepted Manuscript* or any consequences arising from the use of any information it contains.

Table of Contents



A hierarchical porous CNF membrane with robust mechanical properties, exhibiting intriguing shape memory property and efficient protein adsorption performance.



Journal Name

ARTICLE

Hierarchical porous carbon nanofibrous membranes with enhanced shape memory property for effective adsorption of proteins

Received 00th January 20xx,
Accepted 00th January 20xx

DOI: 10.1039/x0xx00000x

www.rsc.org/

Gang Fan ^{a,‡}, Jianlong Ge ^{b,‡}, Hak-Yong Kim ^c, Bin Ding ^{a,b,*}, Salem S. Al-Deyab ^{d,*},
Mohamed El-Newehy ^{d,e}, and Jianyong Yu ^b

Designing and fabricating hierarchical porous carbon nanofibrous (CNF) membranes with good mechanical properties is an attractive and challenging work for next generation of functional separation materials. Here, we demonstrate a novel strategy to create a heterostructured CNF membrane with multiscale pores via multicomponent electrospinning and nano-doping method. The resultant membrane exhibits an intriguing shape memory property, which can be bended to a radius < 100 μm without any fracture and recover from the deformation rapidly. Besides that, the carbonaceous nanofibrous membrane is quite soft like the polymer based wrapping paper. Such robust mechanical properties may be attributed to the “plasticizer” effect of the doped SiO₂ nanoparticles and the protogenetic graphitized carbon layers in carbon matrix. More interesting, benefitting from the functional nitrogenous groups and the hierarchical porous structures, these CNF membranes possess a high adsorption capacity for target protein molecules and high water permeability (15202 ± 1927 L m⁻² h⁻¹ under 3 kPa driven pressure), which is an order of magnitude higher than the commercial polymer based affinity membranes. As this technology is effective and easy to operate, more multifunctional CNF based nanoscale materials could be developed for the next generation of high efficient proteins separations.

Introduction

Carbon nanofiber (CNF) as a typical nanoscale carbon based material is well known for its high temperature resistance, good chemical stability, excellent electrical conductivity, and large specific surface area.^{1,2} Benefiting from these advantages, various CNF based materials with functional interfaces and designed structures have been developed for different applications, such as energy storage electrodes, catalyst carriers, separation membranes and adsorbents.³⁻⁶ Until now, much efforts have been made to synthesis CNF materials, including the substrate method, chemical vapor deposition, vapor growth method, which are quite complex and hard to be scalable.⁷⁻⁸ Alternatively, electrospinning method has become a powerful and highly versatile technique to fabricating both organic and inorganic nanofibrous materials, as the electrospun nanofibers possess merits of extremely high aspect ratio, tunable structures and ease of scalable synthesis from various precursor

polymers.^{2,9,10}

Presently, pharmaceutical proteins have become major contributors in immunodiagnostics, immunotherapy, and scientific research.^{11,12} However, the quality and yield of protein products are not able to meet the demand of market. Thus, much efforts have been taken to develop an effective and low cost approach to produce the high qualified proteins. Therefore, the electrospun CNF membranes has been developed as a promising candidate for high efficient protein separation owing to its high surface area, easy to be functionalized and chemical stability.¹³ However, in the conventional CNFs, most of the pores are micropores (pore size < 1 nm), which are invalid for the entrance of protein molecules (most are in the range of 1~100 nm).¹⁴ As a result, the adsorption capacity of CNFs for proteins is quite difficult to be improved, limiting the practical use of CNFs in proteins separation. More importantly, due to the brittle instinct of carbon compare with polymer based membranes, these CNF membranes often suffer from the low mechanical properties, which are essential for a separation membrane to be packed into devices.¹⁵ To date, there are only a few literatures report their efforts on fabrication of self-standing CNF membranes.¹⁶⁻²⁰ However, these self-standing CNF membranes are still brittle and hard to recover from the deformations. Therefore, the enhancement of mechanical property of CNF membrane with more valid pores is a critical issue for its practical application in proteins separation.

Here, in this contribution, we demonstrate a novel strategy to fabricate a hierarchical porous CNF membrane with enhanced mechanical properties via multicomponent electrospinning, nano-doping method. In addition, an in situ nitrogen-doping approach was taken by reusing the emitted gases from the carbonization of PAN to activate the surface of CNF. The resultant SiO₂@CNF membrane

^a State Key Laboratory for Modification of Chemical Fibers and Polymer Materials, College of Materials Science and Engineering, Donghua University, Shanghai, 201620, China. Email: binding@dhu.edu.cn

^b Key Laboratory of Textile Science & Technology, Ministry of Education, College of Textiles, Donghua University, Shanghai 201620, China.

^c Department of BIN Fusion Technology, Chonbuk National University, Jeonju 561-756, Republic of Korea.

^d Petrochemical Research Chair, Department of Chemistry, College of Science, King Saud University, Riyadh 11451, Saudi Arabia. ssdeyab@ksu.edu.sa

^e Department of Chemistry, Faculty of Science, Tanta University, Tanta 31527, Egypt.

† Electronic Supplementary Information (ESI) available: The in situ SEM images, tensile curves, movies S1 and S2. See DOI: 10.1039/x0xx00000x

‡ These authors contributed equally to this work.

was mechanical robust with an intriguing softness and shape memory behaviour like a polymer based membrane, which may be attributed to the presence of SiO₂ nanoparticles and graphitized carbon layers in carbon matrix. Besides that, the SiO₂@CNF membrane exhibited a significantly improved adsorption capacity for bull serum albumin molecules and a high water permeability. Moreover, a possible mechanism for the enhanced protein adsorption performance is also clarified.

Experimental

Materials

Polyacrylonitrile (PAN, Mw = 90 000) was purchased from Spectrum Chemicals & Laboratory Products Co., Ltd, USA. Dimethylformamide (DMF) was commercially obtained from Shanghai Chemical Reagents Co., Ltd., China. SiO₂ nanoparticles (diameter of particles, 7-40 nm), bovine serum albumin (BSA), lysozyme (Lys), NaH₂PO₄ and Na₂HPO₄ were purchased from Aladdin Chemistry Co. Ltd, China. Ultrapure water was purified by using a Heal-Force system. All chemicals were of analytical grade and were used as received without further purification.

Fabrication of precursor nanofibers

The concentration of PAN in solutions was fixed at 10 wt% and the content of SiO₂ nanoparticles relative to the polymers were adjusted to 0, 5, 10 and 20 wt%. To prepare the solutions, an appropriate amount of SiO₂ nanoparticles were firstly dispersed in DMF and ultrasonicated for 2 h by using a sonication bath. After that, PAN powder was added into the nanoparticles suspension to form a mixture and be stirred vigorously for another 8 h at room temperature to ensure the polymer was completely dissolved. The subsequent electrospinning process was carried out by using the DXES-3 spinning machine (SOF Nanotechnology Co., Ltd., China). Before that, the as-prepared solution was ultrasonicated again for another 2 h to ensure the uniformly dispersion of SiO₂ nanoparticles in fibers. The feed rate of solutions was set at 1.5 mL h⁻¹. As a high voltage of 25 kV was applied to the needles, numerous continuous nanofibers were generated. These nanofibers were collected as a membrane on a grounded metallic rotating roller coated with copper mesh, and the tip to collector distance was fixed at 20 cm. The temperature and humidity for electrospinning were controlled at 25°C and 50 ± 5%.

Carbonization of CNFs

The as-obtained precursor fibers were firstly dried at 60°C for 1h in vacuum to remove the remained solvent and then pre-calcined in an air cycling oven at 280°C for 2 h with external tension. Subsequently, the thermosetting stabilized fibrous membranes were sandwiched between two pieces of graphite plates and annealed under a flowing of high purity nitrogen (99.999%) at 850°C for 120 min with the heating rate of 2°C min⁻¹. The outlet of gases was sealed with a water bath to increase the resident time of emitted gases containing NH₃ in the calcination tube during carbonization for the nitrogen-doping. Products with different initial SiO₂ contents of 5, 10 and 20 wt% were labelled as SiO₂@CNF-5, SiO₂@CNF-10 and SiO₂@CNF-20, respectively. For comparative studies, the pristine CNF membranes were also prepared in the same procedure.

Proteins adsorption performance evaluation.

In this study, both the BSA (negatively charged at the pH of 7.5) and Lys (positively charged at the pH of 7.5) were chosen as the model proteins to test the proteins adsorption performance of the relevant CNF membranes. Protein solutions with different concentrations at a fixed pH value of 7.5 were prepared using phosphate buffer solution. For the static adsorption evaluation, 80 mg of the as-prepared CNF membranes were immersed in 10 mL of the protein solutions for 12 h. After that, liquid from each sample was collected and the protein concentration was determined by using ultraviolet-visible (UV-vis) spectrophotometer. The equilibrium adsorption amount was calculated from the difference between initial and final protein concentrations of solutions, using the following equation: $Q = V(C_i - C_f)/m$, where Q is the adsorptive capacity (mg g⁻¹), V is the volume of the testing solution (mL), C_i and C_f is the initial and final concentration of proteins in solutions (mg mL⁻¹), and m is the dry weight of the membranes (g). The breakthrough curve measurement was further performed to evaluation the dynamic adsorption performance. Circular membranes with a diameter of 15 mm were packed and a total thickness of ~2 mm were sandwiched into a plastic filter holder vertically placed on the horizontal position. 32 mL of BSA solution (1 mg mL⁻¹) was loaded into a syringe and permeate through the membrane under the drive of a syringe pump at a flow speed of 0.1 mL min⁻¹. The outlet solutions was collected at different volume, and tested the concentration of BSA, so that a breakthrough curve could be plotted. For water permeability testing, the SiO₂@CNF membranes with diameter of 40 mm were packed into a filtration devices and the driven pressure were maintained by using a vacuum pump.

Characterization

Morphology of all samples was examined by using a field emission scanning electron microscope (FE-SEM, S-4800, Hitachi Ltd., Japan) operating at 5 kV. The characterizations of nanostructures, selected area electron diffraction (SAED) and energy dispersive X-ray spectroscopy (EDX) were performed on a field emission transmission electron microscopy (FE-TEM, JEM-2100F, JEOL Ltd., Japan). An automatic adsorption system (ASAP 2020, Micromeritics Co., USA) was employed to collect the N₂ adsorption-desorption isotherms. The porous structures were analysed by using the 2-dimensional nonlocal density functional theory (2D-NLDFT) method and Horvath-Kawazoe (HK) method. The Brunauer-Emmet-Teller (BET) surface area was calculated from the N₂ isotherm ranging from 0.05 to 0.35 of relative pressure. Raman spectrum were obtained by using a micro-Raman spectroscopy system (inVia-Reflex, Renishaw, Co., UK). The phase structures of samples were studied via a X-ray diffraction (XRD) (D/Max-2550 PC Rigaku Co., Japan, Cu K α , λ =1.5406 Å). The softness of membranes were evaluated by a softness tester (RRY-1000, Hangzhou Qingtong & Boke Automation Technology Co., Ltd., China) according the ASTM D 2923-95. A tensile tester (XQ-1C, Shanghai New Fiber Instrument Co., Ltd., China) was used to character the tensile mechanical property of the membranes. Water contact angles (WCA) (3 μ L) measurement was performed by using a contact angle goniometer Kino SL200B. The UV-vis spectra were obtained via an Idea optics PG 2000pro fiber-optic spectrometer (Idea Optics Technology Ltd., China) scanning from 180 to 1180 nm at room temperature.

Results and discussion

The FE-SEM images shown in Fig. 1 demonstrate the morphologies

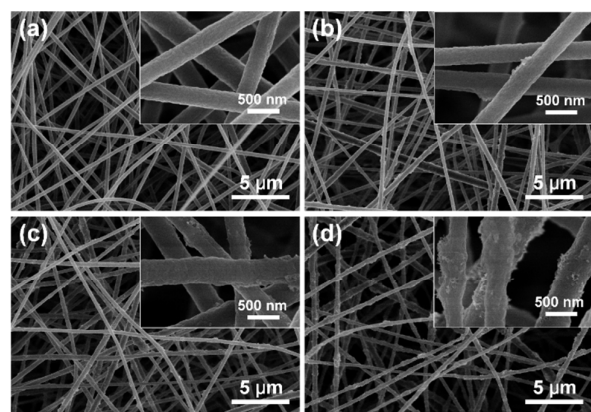


Fig. 1 FE-SEM images of the PAN nanofibers with different concentration of SiO₂ nanoparticles: (a) 0, (b) 5, (c) 10 and (d) 20 wt%. Inset pictures are the corresponding high magnified SEM images.

of precursor nanofibers with different SiO₂ nanoparticles contents. It can be found that in all samples, the fibers possessed a high aspect ratio and randomly deposited network like structures. Dimensional analysis of these FE-SEM images shows that the diameter of relevant precursor fibers were about 336 ± 35 , 342 ± 40 , 359 ± 41 , and 373 ± 45 nm, respectively, indicating a tiny change with the increment of SiO₂ nanoparticles. Meanwhile, high magnified images shows that the roughness the fibers were increased significantly and more beads were appeared with the increment of SiO₂ contents. As for the reasons, on

one hand, the semi-conductor SiO₂ decreased the conductivity of solutions, which cause more bead appearance as previous studies reported.^{21, 22} On the other hand, the aggregated nanoparticles also contributed to the formation of the beads, which could be utilized for the construction of hierarchical structures on the surface of fibers.

Upon calcination, the organic component of precursor fibers gradually converted to carbon with partially burned off and left the inorganic SiO₂ nanoparticles in situ unchanged, finally a hierarchical roughness formed on the surface of fibers. FE-SEM images shown in Fig. 2 demonstrate that the uniform fibrous morphology and high aspect ratio of precursor fibers were well inherited by relevant CNFs. It can be find that all the CNFs were well separated without obvious agglomeration, the average diameters of CNFs reduced to 226 ± 22 , 235 ± 30 , 263 ± 47 , and 274 ± 40 nm, respectively, owing to the shrinkage and burn off of organics during carbonization. As expected, there were numerous bulges presented on the surface of fibers, confirming the successfully construction of hierarchical roughness. Interestingly, with the increment of SiO₂ loadings, more clusters appeared on the surface of CNFs, which could be attributed to the aggregation of nanoparticles. It should be noted that these clusters were effectively bonded by the carbonized layer on the surface of SiO₂ nanoparticles.

To verify the hierarchical structures of CNF membranes, N₂ adsorption-desorption measurements at 77 K was carried out to investigate the porous texture of the as-prepared CNF membranes with different contents of SiO₂ nanoparticles. The isotherms shown in Fig. 3a demonstrate the adsorption behaviours of micropore filling, monolayer adsorption, multilayer adsorption and capillary condensation.²³ As we can see, for pristine CNF there was a rapid adsorption below $P/P_0 < 0.1$ and an adsorption plateaus over the region of $0.1 < P/P_0 < 0.9$, indicating the dominant position of micropores in CNFs. Interestingly, with the addition of SiO₂

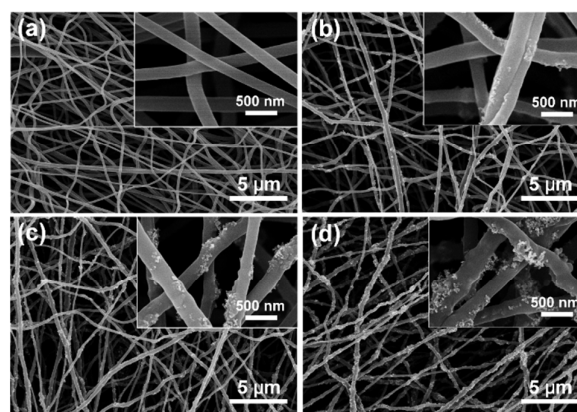


Fig. 2 FE-SEM images of the carbon nanofibers derived from the precursor fibers with different concentration of SiO₂ nanoparticles: (a) 0, (b) 5, (c) 10 and (d) 20 wt%. Inset pictures are the corresponding high magnified SEM images.

nanoparticles, the N₂ adsorption in the range of $0.1 < P/P_0 < 0.9$ increased, and the area of hysteresis loops was enlarged, which suggesting the enhancement mesopores.^{24, 25}

Furtherly, quantitatively analysis were performed to obtain accurate information of pore volume and pore size distribution. Fig. 3b demonstrates the pore size distribution curves of the relevant CNF membrane based on the 2D-NLDFT model and HK model.^{26, 27} It can be find that for pristine CNF the distribution peaks were mainly in the region of micropores (0.5-1 nm), and with the increment of SiO₂ contents, polydisperse peaks centred in the range of mesopores (2-20 nm) appeared, confirming that the pore size had been enlarged. Table 1 give a summary of detailed parameters of pore structures, by which we can see that the surface area of mesopores increased from 32 to 115 m² g⁻¹ and the fraction to the total surface area increased from 8.3 to 43.2%. Additionally, the total volume and mesopore volume fraction were both significantly enhanced, suggesting the effect of SiO₂ nanoparticles on improving the mesopore volume.

To investigate the hierarchical structures, fractal analysis was also carried out. The fractal dimensions (D) of CNFs with different content of SiO₂ nanoparticles were calculated based on the N₂ adsorption isotherms by using a modified Frenkel-Halsey-Hill (FHH) model.²⁸⁻³⁰ (see more in Supporting information) As Fig. 4 presented, the FHH plots of CNFs demonstrate distinct differential slopes in the high coverage region. As a result, the D values of CNF membranes without and with SiO₂ nanoparticles were about 2.982, and 2.830, respectively, suggesting a typical surface fractal feature. Simultaneously, the D values decrease obviously with the presence of SiO₂ nanoparticles, indicating the enhancement of mesoporous structures.^{29, 31} This phenomenon could be ascribed to the formation of clusters of SiO₂ nanoparticles on the surface fibers, which was agree with the morphologies observed in Fig. 2.

The nanostructures of CNFs were systematically analysed by using Raman spectra, XRD, FT-IR, and TEM to find out the effect of SiO₂ nanoparticles on the evolution of nanotextures. Fig. 5 compares the Raman spectrum of relevant CNFs derived from precursor fibers with different contents of SiO₂ nanoparticles. As can be seen that, all samples presented the D band (1345 cm⁻¹) corresponding to the disordered carbon and G band (1583 cm⁻¹) demonstrating the sp² ordered carbon. In addition, the degree of

Table 1 The summary of pore structure parameters of CNFs.

Samples	S_{BET}^a ($\text{m}^2 \text{g}^{-1}$)	S_{meso}^b ($\text{m}^2 \text{g}^{-1}$)	SF_{meso}^c (%)	V_{total}^d ($\text{cm}^3 \text{g}^{-1}$)	V_{meso}^e ($\text{cm}^3 \text{g}^{-1}$)
Pristine CNF	383	32	8.3	0.22	0.024
SiO_2 @CNF-20	266	115	43.2	0.31	0.234

^a Total surface area was calculated by the Brunauer-Emmett-Teller (BET) method. ^b Mesoporous surface area was calculated by the Barret, Joyner, and Halenda (BJH) method. ^c SF_{meso} indicates the surface area fraction of mesopores. ^d Total pore volume was estimated was calculated at $P/P_0=0.99$. ^e V_{meso} was calculated by the BJH method.

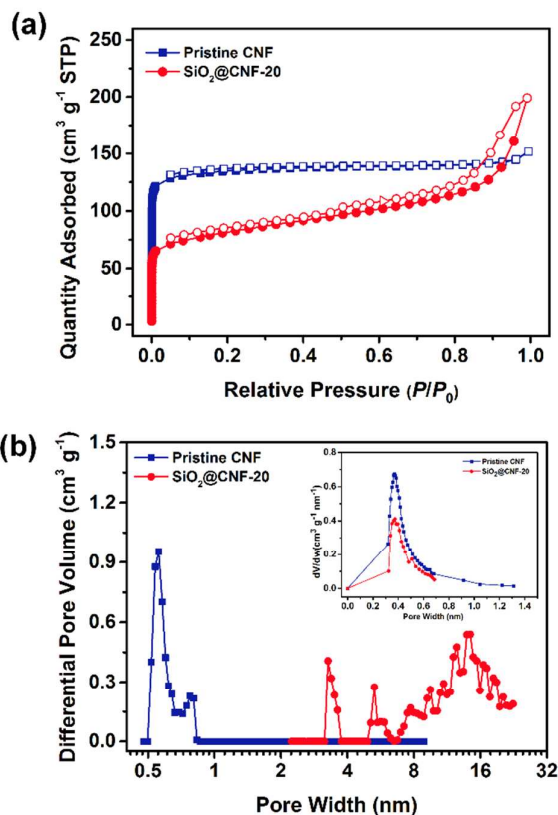


Fig. 3 (a) N_2 adsorption-desorption isotherms and (b) 2D-NLDFT pore size distribution curves of relevant CNF membranes. Inset picture is the corresponding HK pore size distribution curves.

crystallinity of carbon (R) were estimated from the ratios of I_G/I_D .³² It is found that for CNFs derived from precursor fibers with SiO_2 concentration of 0, 5, 10 and 20 wt%, the corresponding R values were 0.941, 0.970, 0.977 and 0.979, respectively, demonstrating a slight increment of graphitization with the addition of SiO_2 nanoparticles. This may be attributed to the promotion of graphitization caused by SiO_2 . XRD patterns of pristine CNF and relevant SiO_2 @CNF shown in Fig. 6 depicts two broad peak at approximately 24° and 43° corresponding to the (002) and (100) diffraction planes of graphite, suggesting the presence of carbon.³³ It is worth to note that the characteristic diffraction peak of carbon and SiO_2 are quite closed (~ 23 - 25°); as a result the diffraction peak of

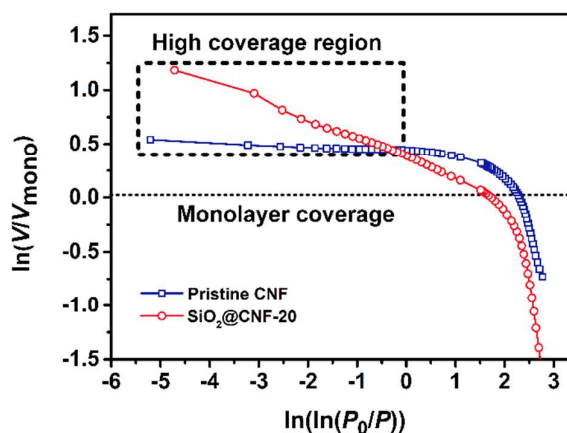


Fig. 4 Plots of $\ln(V/V_{\text{mono}})$ against $\ln(\ln(P_0/P))$ reconstructed from the N_2 adsorption isotherms obtained from relevant CNF membranes.

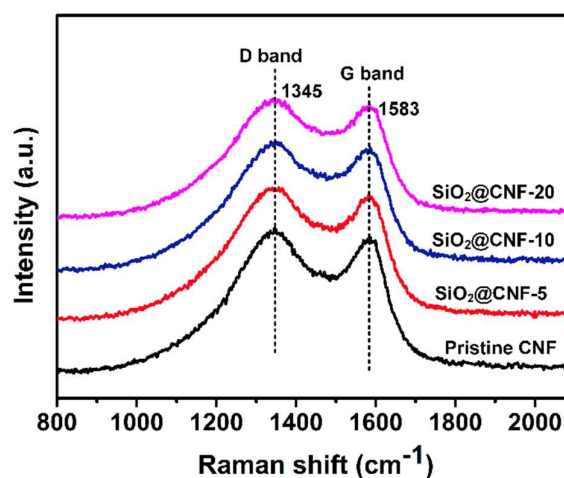


Fig. 5 Raman spectrum of CNFs derived from precursor fibers with different content of SiO_2 nanoparticles.

SiO_2 was overlapped by that of carbon.^{34, 35} The FT-IR spectrum of pristine CNF and relevant SiO_2 @CNF were presented in Fig. 7a. As observed from the spectrum, characteristic peaks present at ~ 630 , 880, 1058, 1623 and 3440 cm^{-1} , corresponding to the $\text{C}\equiv\text{C}$, $\text{Si}-\text{OH}$, $\text{Si}-\text{O}$, $\text{C}-\text{O}$, $\text{C}=\text{C}$, and $\text{N}-\text{H}/\text{O}-\text{H}$ stretch, respectively.^{36, 37} TEM images shown in Fig. 7b, c demonstrate that the amorphous SiO_2 nanoparticles were well dispersed both intra and on the surface of CNFs. And the ordered graphitized carbon layers with d-spacing of 0.41 nm (002) can be recognized in the HRTEM images. The diffraction rings shown in the SAED patterns (Fig. 7d) also confirm the multi-crystalline structure of carbon matrix, which may be beneficial for improving the mechanical properties of CNFs. The EDX analysis was also performed on the SiO_2 @CNF-20 to further verify the presence of SiO_2 and nitrogen in CNFs. The strong peaks in the EDX patterns (Fig. 7e) confirmed the presence of C, Si, O and N, and the TEM element maps (Fig. 4f-i) depict the distinct shape of a fiber, indicating an evenly distribution of these elements in the matrix of CNFs.

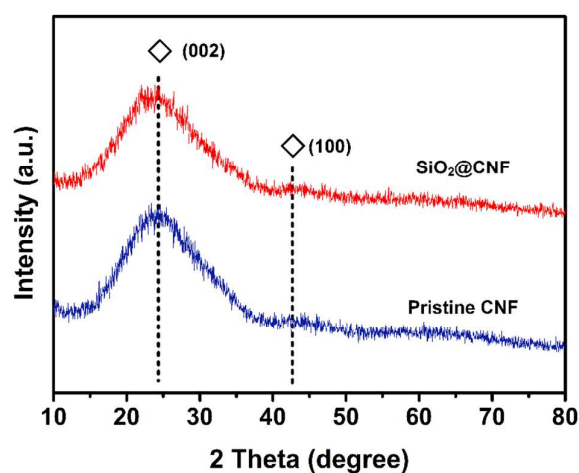


Fig. 6 XRD spectrum of pristine CNF and SiO₂@CNF-20.

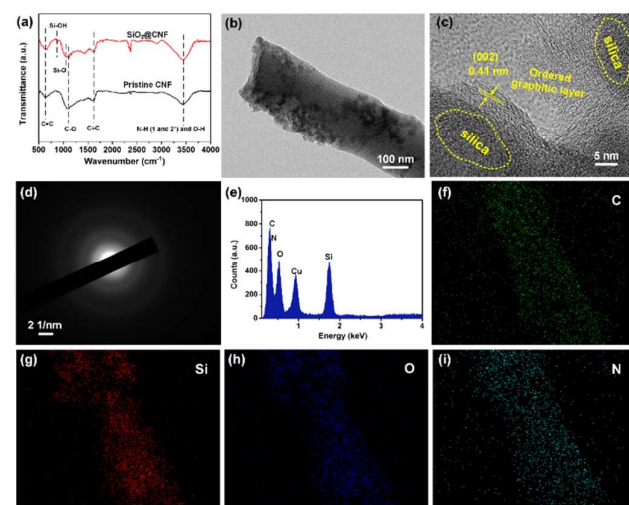


Fig. 7 (a) FT-IR spectra of pristine CNF and SiO₂@CNF. (b) TEM and (c) HR-TEM of SiO₂@CNF-20. (d) SAED pattern of selected a single fiber. (e) EDX spectra of a selected area. (f-i) Elemental mapping of C, Si, O, and N on a single fiber.

The effect of SiO₂ nanoparticles on the mechanical properties of CNF membranes were systematically investigated. Generally, the pristine CNF membranes are quite brittle, which would fracture even under a tiny bending deformation, as shown in Fig. S1. Interestingly, with the introduction of appropriate amount of SiO₂ nanoparticles, the mechanical properties of CNF membranes were improved significantly, and an intriguing shape memory performance was possessed. As shown in Fig. 8a, the stiffness of CNF membranes were decreased with the increment of SiO₂ content, indicating a remarkable enhancement of softness; there into the membrane (stiffness value of ~69 mN) derived from SiO₂@CNF-20 was even softer than the commercial polymer based wrapping paper (stiffness value of ~74 mN). Fig. 8b demonstrate the calculated Young's modulus of relevant CNF membranes based on the representative tensile curves (Fig. S2). As can be seen that the Young's modulus

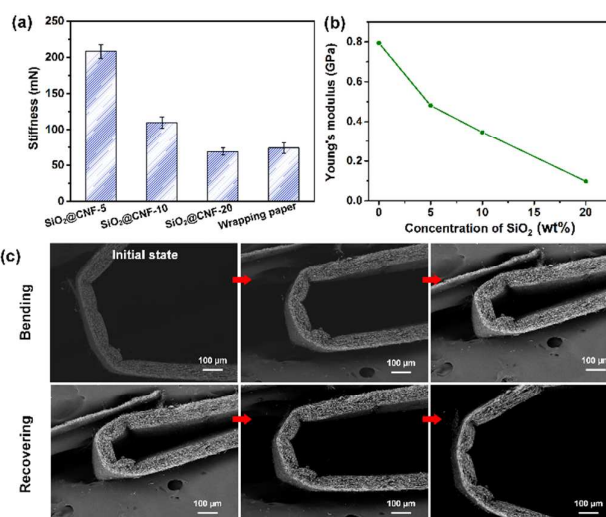


Fig. 8 (a) Stiffness of CNF membranes with different content of SiO₂ nanoparticles. (b) Corresponding Young's modulus as a function of SiO₂ nanoparticle loading. (c) In situ SEM observations of the bended SiO₂@CNF-20 membrane and recovery, focusing on a small piece (< 2 mm).

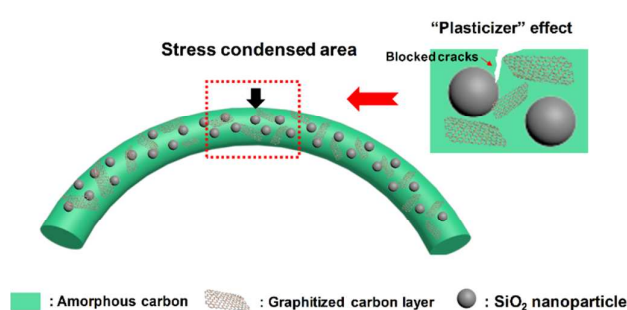


Fig. 9 Schematic illustration showing the structure and plausible mechanism for the mechanical enhancement of SiO₂@CNFs.

were evidently decreased with the increase of SiO₂ nanoparticles content, confirming the improvement of softness. Furthermore, in order to verify the shape memory property of SiO₂@CNF membranes in the micro scale, the in situ SEM characterization was performed on a tiny piece of relevant membranes. As seen in Fig. 8c, a piece of SiO₂@CNF-20 membrane (length < 2 mm) was placed between two parallel plates, and the SEM observations were conducted at a certain bending deformation. The result showed that this membrane can be bended down to a circle with radius < 100 μm without any fracture, and it can recover from the deformations soon. The high magnification SEM images shown in Fig. S3 demonstrated that the single fibers could keep intact after extreme bending deformations. In addition, the relevant SiO₂@CNF membrane could maintain its robust shape memory property both in the flames and liquid nitrogen, which can be seen in Supporting Information Movies S1 and S2.

Based on the systematically studies of the morphology and nanostructures of relevant CNF, a probable mechanism of the enhancement of mechanical properties were proposed. Due to the good continuity of fibers and closed-packed structure of CNF

membranes, the external stress on the membrane would finally result in the bending deformation of a single fibers. For pristine CNF the stress would concentrate on the bending area and generate cracks, these cracks extended rapidly without any blocking, finally causing the fracture of fibers. As for $\text{SiO}_2@\text{CNF}$ derived from precursor fibers with appropriate content of SiO_2 , these evenly distributed nanoparticles and protogenetic graphitized carbon layers in the carbon matrix acted as “plasticizer” to scatter the concentrated stress, as shown in Fig. 9, so that the propagation of tiny cracks would be inhibited, therefore the structural fracture of CNF membranes would be avoided.

An appropriate hydrophilicity is essential both for the adsorption of protein molecules and the permeation of buffer solutions. Fig. 10a demonstrates that the water contact angle (WCA) of relevant CNF membranes decrease from $36.8 \pm 0.5^\circ$ to $20.6 \pm 0.6^\circ$ with the increment of SiO_2 contents, indicating an remarkable improvement of hydrophilicity. This phenomenon could be attributed to two aspects: (1) there were abundant hydrophilic groups in SiO_2 (Si-OH) and carbon (N-H), which would definitely enhance the hydrophilicity; (2) the intrinsic hydrophilicity of the fiber surface were further enhanced by the hierarchical roughness according to the Cassie model.³⁸ Fig. 10b demonstrate the water permeability of the $\text{SiO}_2@\text{CNF}$ membranes at a fixed driven pressure of 3 kPa. As expected, the membranes with higher concentration of nanoparticles possessed obviously higher flux, and the $\text{SiO}_2@\text{CNF}-20$ exhibited a flux of $15202 \pm 1927 \text{ L m}^{-2} \text{ h}^{-1}$, which is an order of magnitude higher than the commercial polymer based affinity membranes.³⁸ This phenomenon mainly benefited from the improved hydrophilicity and hierarchical roughness channels, which enhanced the water capillary effect of the membranes according to the Hagen-Poiseuille theory.³⁹

Subsequently, the protein adsorption performance was studied by using a batch wise adsorption method at the room temperature. As described in Fig. S4, it can be found that the saturated adsorption capacity of BSA on CNF membranes increased obviously with the inclusion of SiO_2 nanoparticles. The $\text{SiO}_2@\text{CNF}-20$ possessed the highest adsorption capacity of $30 \pm 0.9 \text{ mg g}^{-1}$, which was remarkable enhanced than the pristine CNF. Furthermore, a plausible mechanism for the enhanced adsorption is proposed. Firstly, the adsorption of BSA was carried out in a buffer solution with pH of 7.5, which was above the isoelectric point 4.7 of BSA molecules; as a result, the proteins were negatively charged. Considering that the N-H groups on the surface of nitrogen-doped CNFs were positively charged in buffer solutions, thus the electrostatic attraction could be considered as a main contributor for the BSA adsorption; it could be proven by the anti-adsorption behaviour of the positively charged Lys, which exhibited quite low adsorption capacity on the CNF membrane (Fig. 10c). Besides that, the hydrophobic interaction between carbon and the proteins, and the physico-chemical adsorption of BSA should also be considered; because there are multiple adsorptive sites of BSA derived from several amino acids such as cysteine, tyrosine and tryptophan, by which hydrogen bonding and electro-active amino acids are also likely to present.⁴⁰ Secondly, with addition of SiO_2 nanoparticles, the dense texture of carbon matrix was loosened, which could open up the pores, and the hierarchical roughness structures were also formed on the surface of fibers. All these above were benefit for increase the valid interior surface exposed to the proteins for adsorption, in particular that of mesoporous, which has been confirmed above. Consequently, the good permeability and high adsorption capacity of the $\text{SiO}_2@\text{CNF}$ membrane made it a promising affinity membrane for continuous protein separation. Thus, the dynamic adsorption performance evaluation was further performed on the $\text{SiO}_2@\text{CNF}-20$ membranes. Figure 10d shows a typical breakthrough curve of the dynamic adsorption. The increment of the outlet concentration was slow

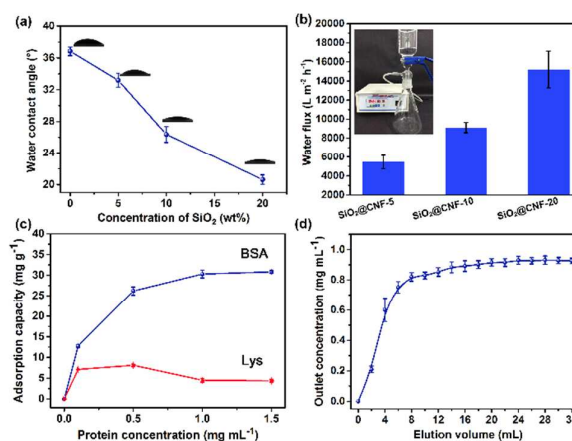


Fig. 10 (a) Hydrophobicity and (b) Water permeability of relevant $\text{SiO}_2@\text{CNF}$ membranes. Inset is the filtration device. (c) Equilibrium adsorption curves of $\text{SiO}_2@\text{CNF}-20$ membranes for BSA and Lys. (d) Break through curve of BSA through the $\text{SiO}_2@\text{CNF}-20$ membranes.

outlet concentration was slow and reached the feed concentration until the elution volume was $\sim 24 \text{ mL}$ with a saturation dynamic adsorption capacity of $\sim 22.8 \text{ mg g}^{-1}$. As an ideal affinity membrane should capture 90% of its saturated capturing capacity when the outlet concentration reach 10% of the feed concentration.³⁸ For the resultant $\text{SiO}_2@\text{CNF}-20$ membrane, 66% of its saturation adsorption capacity could be gained when the outlet concentration reached 0.6 mg mL^{-1} , which was less than 90% of the saturation adsorption capacity. This phenomenon could be ascribed to the wide pore size distribution of the membrane, resulting a broadened mass transfer rate inside the membranes. To enhance the practical application performance of $\text{SiO}_2@\text{CNF}$ based protein separation membranes, the pore structures and activity of interfaces should be further optimized by regulating the morphology of doped nanoparticles or functional groups on the surface of fibers.

Conclusions

In this study, we have demonstrated a novel strategy for the fabrication of CNF membrane with hierarchical porous structures based on the multicomponent electrospinning and in situ nanodoping method. The as-prepared CNF membrane possessed robust mechanical properties, which is even softer than the polymer based wrapping paper and show an intriguing shape memory performance. A plausible mechanism of the enhancement of mechanical properties was also proposed. The embedded SiO_2 nanoparticles and ordered graphitized carbon layers in the carbon matrix acted as the “plasticizer” for the external stress, endowing the CNFs a robust mechanical stability under extreme bending deformations. In addition, the doped nitrogen on the surface of fibers increased the binding sites for proteins, and the hierarchical porous structures with mesoporous surface area of $115 \text{ m}^2 \text{ g}^{-1}$ derived from SiO_2 nanoparticles enhanced the valid interface for protein adsorption. As a result, the $\text{SiO}_2@\text{CNF}$ membranes possessed a significantly improved adsorption performance for BSA molecules. With the good mechanical properties, high water permeability, and moderate protein adsorption capacity, the $\text{SiO}_2@\text{CNF}$ membranes can be effectively used for continuous proteins separation, which is essential for the industrial production. We anticipate that this work could not only provide a general strategy to fabricate the hierarchical porous CNF membranes for BSA adsorption, but also open up a new route to the design and development of next generation of

multifunctional CNF based nanoscale materials for various applications.

Acknowledgements

This project was funded by the National Plan for Science, Technology and Innovation (MAARIFAH), King Abdulaziz City for Science and Technology, Kingdom of Saudi Arabia, Award Number (11-NAN1915-02).

Notes and references

- H. Kim, D. H. Seo, S. W. Kim, J. Kim and K. Kang, *Carbon*, 2011, **49**, 326-332.
- M. Inagaki, Y. Yang and F. Y. Kang, *Adv. Mater.*, 2012, **24**, 2547-2566.
- C. Xia, W. Chen, X. B. Wang, M. N. Hedhili, N. N. Wei and H. N. Alshareef, *Adv. Energy Mater.*, 2015, **5**.
- W. Guanjie, J. Minghua, F. Xinzhuang, L. Jianguo and Y. Chuanwei, *J. Power Sources*, 2015, **287**, 81-86.
- M. H. Tai, P. Gao, B. Y. L. Tan, D. D. Sun and J. O. Leckie, *Acs Appl. Mater. Interfaces*, 2014, **6**, 9393-9401.
- L. Hua, C. Chang-Yan, W. Fang-Fang, H. Pei-Pei, S. Yong-Bin, J. Lei and S. Wei-Guo, *J. Mater. Chem. A*, 2014, **2**, 3557-3562.
- A. Roethlisberger, M. Seita, A. Reiser, E. Shawat, R. Spolenak and G. D. Nessim, *Carbon*, 2013, **63**, 498-507.
- W. Huiyao and J. J. Moore, *Carbon*, 2012, **50**, 1235-1242.
- Q. Wen, J. C. Di, Y. Zhao, Y. Wang, L. Jiang and J. H. Yu, *Chem. Sci.*, 2013, **4**, 4378-4382.
- C. C. Lai and C. T. Lo, *RSC Adv.*, 2015, **5**, 38868-38872.
- C. Katz, L. Levy-Beladev, S. Rotem-Bamberger, T. Rito, S. G. D. Rudiger and A. Friedler, *Chem. Soc. Rev.*, 2011, **40**, 2131-2145.
- Y. P. Li, T. Y. Lin, Y. Luo, Q. Q. Liu, W. W. Xiao, W. C. Guo, D. Lac, H. Y. Zhang, C. H. Feng, S. Wachsmann-Hogiu, J. H. Walton, S. R. Cherry, D. J. Rowland, D. Kukis, C. X. Pan and K. S. Lam, *Nat. Commun.*, 2014, **5**.
- S. Schneiderman, L. F. Zhang, H. Fong and T. J. Menkhaus, *J. Chromatogr. A*, 2011, **1218**, 8989-8995.
- S. Singh, A. Singh, V. S. S. Bais, B. Prakash and N. Verma, *Mater. Sci. & Eng. C-Mater. Biol. Appl.*, 2014, **38**, 46-54.
- F. M. Gao, *J. Appl. Phys.*, 2012, **112**.
- C. Ma, Y. J. Li, J. L. Shi, Y. Song and L. Liu, *Chem. Eng. J.*, 2014, **249**, 216-225.
- C. L. Lai, P. Kolla, Y. Zhao, H. Fong and A. L. Smirnova, *Electrochim. Acta*, 2014, **130**, 431-438.
- C. L. Lai, Z. P. Zhou, L. F. Zhang, X. X. Wang, Q. X. Zhou, Y. Zhao, Y. C. Wang, X. F. Wu, Z. T. Zhu and H. Fong, *J. Power Sources*, 2014, **247**, 134-141.
- F. Zhang, C. Z. Yuan, J. J. Zhu, J. Wang, X. G. Zhang and X. W. Lou, *Adv. Funct. Mater.*, 2013, **23**, 3909-3915.
- B. A. Zhang, Y. Yu, Z. D. Huang, Y. B. He, D. Jang, W. S. Yoon, Y. W. Mai, F. Y. Kang and J. K. Kim, *Energy Environ. Sci.*, 2012, **5**, 9895-9902.
- Y. Si, J. Yu, X. Tang, J. Ge and B. Ding, *Nat. Commun.*, 2014, **5**.
- X. M. Tang, Y. Si, J. L. Ge, B. Ding, L. F. Liu, G. Zheng, W. J. Luo and J. Y. Yu, *Nanoscale*, 2013, **5**, 11657-11664.
- R. Balgis, T. Ogi, A. F. Arif, G. M. Anilkumar, T. Mori and K. Okuyama, *Carbon*, 2015, **84**, 281-289.
- Z. Le-Sheng, L. Wei, C. Zhi-Min and S. Wei-Guo, *J. Phys. Chem. C*, 2009, **113**, 20594-20598.
- B. Fotoohi and L. Mercier, *Microporous and Mesoporous Mat.*, 2015, **211**, 38-48.
- A. V. Neimark, Y. Lin, P. I. Ravikovitch and M. Thommes, *Carbon*, 2009, **47**, 1617-1628.
- J. Jagiello and J. P. Olivier, *J. Phys. Chem. C*, 2009, **113**, 19382-19385.
- A. P. Perissinotto, C. M. Awano, D. A. Donatti, F. S. de Vicente and D. R. Vollet, *Langmuir*, 2015, **31**, 562-568.
- G. Orsini and V. Tricoli, *J. Mater. Chem.*, 2012, **22**, 23861-23870.
- M. J. Watt-Smith, K. J. Edler and S. P. Rigby, *Langmuir*, 2005, **21**, 2281-2292.
- B. Sahouli, S. Blacher and F. Brouers, *Langmuir*, 1997, **13**, 4391-4394.
- C. Hu, S. Sedghi, A. Silvestre-Albero, G. G. Andersson, A. Sharma, P. Pendleton, F. Rodriguez-Reinoso, K. Kaneko and M. J. Biggs, *Carbon*, 2015, **85**, 147-158.
- X. Xuezhu, Z. Jian, J. Long, G. Lubineau, S. A. Payne and D. Gutschmidt, *Carbon*, 2014, **80**, 91-102.
- H. Yang, Y. Liu, Q. H. Shen, L. F. Chen, W. H. You, X. M. Wang and J. S. Sheng, *J. Mater. Chem.*, 2012, **22**, 24132-24138.
- M. Guo, B. Ding, X. H. Li, X. L. Wang, J. Y. Yu and M. R. Wang, *J. Phys. Chem. C*, 2010, **114**, 916-921.
- V. Helenius, J. Korppi-Tommola, S. Kotila, J. Nieminen, R. Lohikoski and J. Timonen, *Chem. Phys. Lett.*, 1997, **280**, 325-332.
- Y. Li, B. Li, Y. Fu, S. Lin and Y. Yang, *Langmuir*, 2013, **29**, 9721-9726.
- Z. W. Ma, M. Kotaki and S. Ramakrishna, *J. Membr. Sci.*, 2005, **265**, 115-123.
- Y. Si, Q. Fu, X. Wang, J. Zhu, J. Yu, G. Sun and B. Ding, *Acs Nano*, 2015, **9**, 3791-3799.
- B. B. Prasad, A. Prasad and M. P. Tiwari, *Biosens. Bioelectron.*, 2013, **39**, 236-243.